Path-Loss Characteristics of Urban Wireless Channels

Path-Loss Characteristics of Urban Wireless Channels

Keith T. Herring, Jack W. Holloway, David H. Staelin, *Life Fellow, IEEE*, and Daniel W. Bliss, *Member, IEEE*

***Abstract*—Wireless channel data was collected in Cambridge, Massachusetts for diverse propagation environments over distances ranging from tens of meters to several kilometers using mobile 2.4-GHz transmitters and receivers. The 20-MHz bandwidth signals from eight individually movable van-top antennas were Nyquist sampled simultaneously with 12-bit accuracy. Although path-loss variance for any given link length within single residential/urban neighborhoods was large, single streets typically exhibited path-loss, $\mathrm{L(dB)} = -10\log_{10}(\mathrm{P}_r/\mathrm{P}_t) \cong 10\alpha\log_{10}\mathrm{r} + \mathrm{C}$, where P is the received or transmitted power, r the link-length, α the street-dependent path-loss coefficient, and C the loss incurred at street intersections. Measurements yielded $\alpha \cong 1.5 + 3.2\beta \pm 0.27$ for $2 < \alpha < 5$; β is the fraction of the street length having a building gap on either side. Experiments over links as short as 100 meters indicate a 10-dB advantage in estimating path loss for this model compared to optimal linear estimators based on link length alone. Measured air-to-ground links were well modeled by $\alpha = 2$ for the elevated LOS path, and by stochastic log-normal attenuation for the ground-level scattering environment. These models permit path-loss predictions based on readily accessible environmental parameters, and lead to efficient nodal placement strategies for full urban coverage.**

***Index Terms*—Attenuation, communication channels, data models, fading channels, microwave propagation, multipath channels, multiple-input multiple-output (MIMO) systems, propagation, statistics, urban areas.**

I. Introduction

CONSUMER electronics and other communications systems are increasingly utilizing wireless technology. While protocols such as 802.11b (WiFi) and bluetooth have been implemented for some time, the emergence of multiple-input multiple-output (MIMO) communications [1]–[5] has increased commercial interest. Therefore it is increasingly important to understand the propagation characteristics of environments where this new technology will be deployed [6]. The development of high-performance system architectures and protocols at low-cost depends partly on the accuracy of the channel path-loss models used for planning, for these models determine the requirements for transmitter power, node spacing, and antenna design.

Deterministic path-loss models assume that enough is known about the propagation environment that electromagnetic propagation laws can be used to calculate the power attenuation. Ray tracing plus physical modeling is perhaps the most popular such approach [7]–[12] although deterministic approaches are seldom used because of the difficulty and cost of obtaining high-resolution environment descriptions.

In contrast, empirical models attempt to model path-loss L as obeying a set of equations based on real channel measurements. The most widely used of these include the Stanford University Interim (SUI) [15], Hata [16], [17], and COST-231 models [18]. The equations typically take the form

$$\mathrm{L[dB]} = 10\alpha\log_{10}(\mathrm{r}) + \mathrm{C} \tag{1}$$

where the predicted path-loss L is a function of the link-length r, path-loss coefficient α, and fixed-loss component C. Observed values for α and C are usually calculated using regression analysis across antenna heights, operating frequency, and different macro-environment types, e.g. urban vs. suburban.

In this paper we study the empirical performance of these models based on a large database of real wireless channel data obtained from diverse urban propagation environments. A mobile channel-data collection system was built that includes an eight-channel software receiver and a collection of transmitting WiFi channel sounders [19]. The software receiver synchronously samples the signals from eight individually movable antennas in the 20-MHz band centered at 2.4 GHz. Both air-to-ground and ground-to-ground links were measured for distances ranging from tens of meters to several kilometers throughout the city of Cambridge, MA.

These data sets demonstrate that the average attenuation across frequency within a single macro-environment can vary over 50 dB, suggesting generally large rms errors for empirically based models. In contrast we observe that individual macro-environments can be partitioned into smaller sub-regions of practically relevant size that exhibit more predictable attenuation. These empirical results demonstrate that propagation models based on simple representations of the environment can reduce rms path-loss estimates within such homogeneous subregions by roughly 10 dB for links as short as 100 meters.

Section II introduces the channel measurement system and estimation algorithms. Section III presents the results of the propagation measurements that underlie the propagation model, and Section IV introduces the model itself and illustrates its application to urban streets in comparison to empirical models. Section V presents additional measurements of air-to-ground

Manuscript received August 11, 2008; revised July 08, 2009. First published November 10, 2009; current version published January 04, 2010. This work was supported by the National Science Foundation under Grant ANI-0333902.

K. T. Herring and D. H. Staelin are with the Research Laboratory of Electronics, Massachusetts Institute of Technology (MIT), Cambridge, MA 02139 USA (e-mail: kherring@alum.mit.edu; staelin@mit.edu).

J. W. Holloway was with the Research Laboratory of Electronics, Massachusetts Institute of Technology (MIT), Cambridge, MA 02139 USA. He is currently with the U.S. Marine Corps, Corpus Christi, TX 78419 USA (e-mail: jack.hollloway@gmail.com).

D. W. Bliss is with the Research Laboratory of Electronics, Massachusetts Institute of Technology (MIT), Cambridge, MA 02139 USA and also with MIT Lincoln Laboratory, Lexington, MA 02420 USA (e-mail: bliss@ll.mit.edu).

Color versions of one or more of the figures in this paper are available online at http://ieeexplore.ieee.org.

Digital Object Identifier 10.1109/TAP.2009.2036278

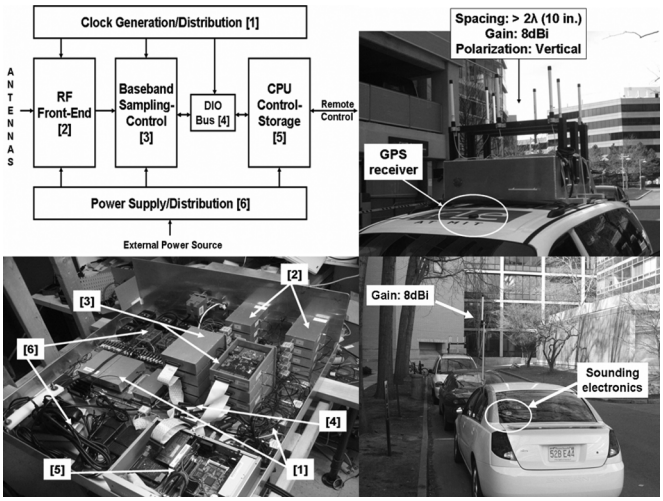

Fig. 1. Overview of the channel-data collection system. Top-left: architecture of eight-channel software receiver; top-right: receiver mounted to van; bottom-left: receiver with case lid removed; bottom-right: transmitting antenna mounted about 1 m above a car. Numbers [1]–[6] relate the receiver block diagram to its photograph.

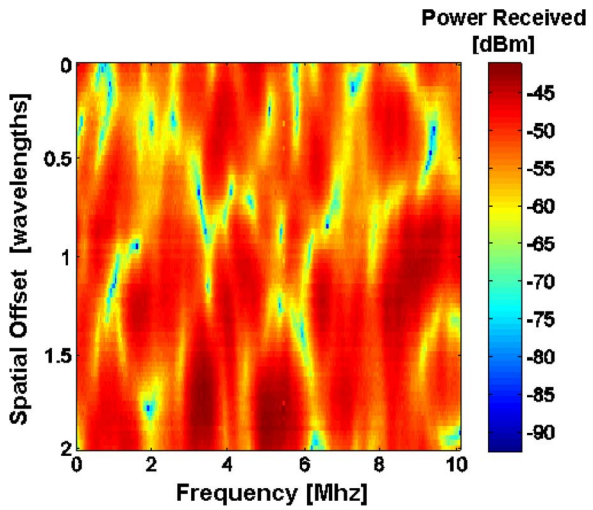

Fig. 2. Illustrative 10-MHz channel power spectrum near 2.422 Ghz obtained from the algorithms applied to data from one antenna as it moved to 40 locations spaced uniformly along a line 2 wavelengths long ($\lambda = 12$ cm).

links, which are a special case of the model, and Section VI summarizes the contributions of the work.

II. Instrumentation and Software

A. Channel-Data Collection System

The Channel-Data Collection System (CDCS) is a set of instrumentation and software that collects large amounts of coherent multi-antenna wireless channel data [19]. The CDCS incorporates an eight-channel software receiver, channel sounder (WiFi transmitter), an array of eight individually movable antenna elements, software packages for system control and database management (distributed across the laptop controller, network, and onboard receiver PC), a GPS tracking system, and infrastructure for system mobility. Fig. 1 displays the major system components.

The software receiver samples the 33-MHz band centered at 2.422 GHz, which includes channel 3 of the 802.11b wireless standard. The receiver synchronously samples this band at a 67-MHz sampling rate at eight configurable antenna elements for 1-msec continuous bursts. Each data burst, called a snapshot, is stored in an on-board PC until transferred to the database for post-collection analysis of the central 10 MHz of the 20-MHz wide Channel 3. The receiver includes the following functional blocks shown in Fig. 1: RF front-end, baseband sampling/control, CPU—control/storage, clock generation/distribution, and power supply. The channel sounding system is a modified ROOFNET node where ROOFNET is an experimental 802.11b/g mesh network developed at MIT CSAIL [20]. The channel sounder continually transmits 802.11b packets with arbitrary payload and duration. The transmitter is battery operated and includes a 1-Watt output amplifier for maximizing experiment range.

B. Channel Extraction and Estimation

The Channel Extractor is a collection of algorithms implemented in MATLAB that estimates the complex channel spectra characterizing the links between the transmitter and each receiver antenna, based on the raw channel data collected by the CDCS. The magnitudes of these complex channel spectral estimates are the base data used in the analysis and experiments that follow. The Channel Extractor software incorporates five functional blocks: matched-filter construction, front-end digital band-pass filtering, detection, time-frequency correction, and channel estimation. This software produces a channel spectral estimate for each snapshot with 33-kHz resolution across only the flat central 10-MHz of the band, which simplified the analysis. Fig. 2 illustrates the received power spectrum estimated by this software for a series of snapshots taken as the transmitter translated linearly 40 times while it moved two wavelengths. The Non-Line-Of-Sight (NLOS) 100-meter links were recorded in a rich outdoor multipath environment.

III. Experiments

The following measurements were carried out across the MIT campus and city of Cambridge, Massachusetts. The multi-antenna receiver was mounted on the roof of a van and the transmitter to a car; see Fig. 1. The receiver antennas were each separated by at least 2 wavelengths (>24 cm) and all antennas elements at both link-ends were vertically polarized 8-dBi omnidirectional units constructed as thin cylinders (see Fig. 1).

A. Macro-Environment Stability

We first consider the performance of empirical path-loss models that predict attenuation, averaged across frequency (10 MHz) and across the 8 antennas, according to (1) using empirically fitted values for α and C observed within that environment type. Fig. 3 displays a scatter plot of power received (dBm) versus link length for a single multi-street residential neighborhood. The transmitter remained in a single location while the receiver traversed neighboring streets within a radius of several city

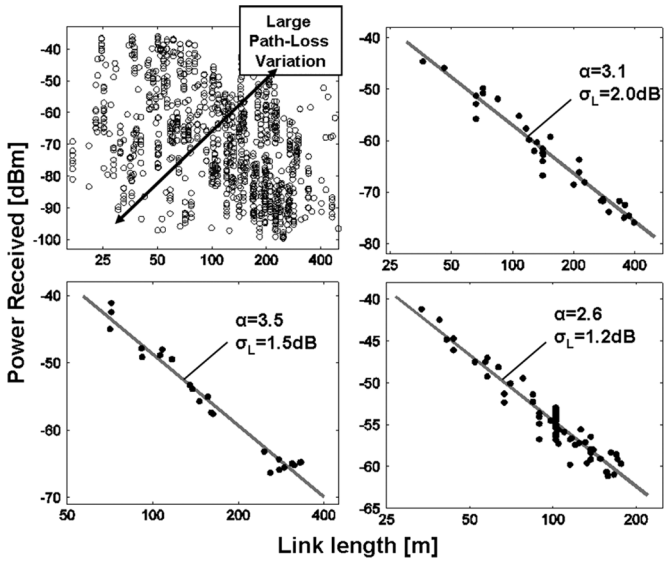

Fig. 3. Path-loss measurements along urban streets. Top-left image: measurements taken within a radius of several blocks within a residential neighborhood. Remaining images: measurements taken along individual streets when the transmitter was hidden around a corner.

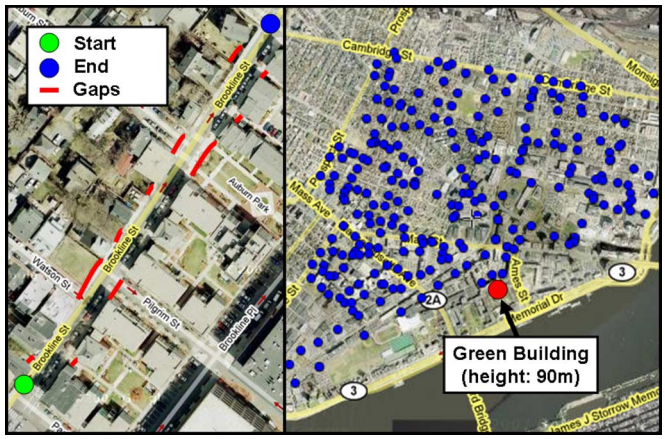

Fig. 4. Measurement environments left: representative street measurement location. Red lines indicate gaps along the street used to calculate β and β'. Right: air-to-ground link measurements for the transmitter mounted on top of the Green Building 90 meters above street level; each blue dot corresponds to a unique receiver location. The image is approximately 2.5 km wide.

blocks. A large variance was observed in the relation between received power and link-length as different neighborhood sections were reached. This suggests that using a single value for α for a particular neighborhood, as is assumed in popular empirical models, can lead to large errors (tens of dB) in path-loss estimates. For links of these lengths ($<$1 km), the numbers and types of objects between transmitter and receiver can vary significantly as a function of direction, thus leading to this result. Since many wireless applications operate over similar link-lengths, it would be desirable to improve this performance.

To improve path-loss predictability, we consider partitioning individual macro-environments into smaller subregions. Specifically, returning to the residential neighborhood, the relative power-attenuation was observed as the receiver moved along single streets within the neighborhood while the stationary transmitter was concealed around a corner. The van housing the receiver was driven down each street while channel snapshots were taken at regular intervals. Fig. 3 displays the power received as a function of link-length along three representative streets. The link-length is measured as the two-dimensional euclidian distance between transmitter and receiver. Given that the transmitter was within 5 meters of the street corner in each measurement location, this distance added less than one meter to the link distance. The path-loss coefficient α associated with each street is estimated as the least-squares linear regression fit to each scatter plot and displayed accordingly. Having tens of samples per street the regression error was less than 0.02α for each street, with α ranging between 2 and 5. In Fig. 3 we observe that the rms error σ_L in the linear path-loss estimator is reduced to a few dB when restricted to these smaller subregions. This leads to the question of how to estimate the proper α for each street.

B. Predicting Path-Loss From Local Environmental Parameters

The analysis in the previous section suggests that path-loss characteristics are generally stationary only within physically homogeneous neighborhoods. We therefore explore the problem of predicting α and C for level urban streets by modeling them as lossy waveguides for which the loss is dominated by the departure of guided rays through gaps between buildings spaced along the street. Natural physical parameters for predicting path-loss are those that characterize these gaps. Fig. 4 displays a satellite image of a representative street and its defined gaps.

To test this hypothesis the streets were characterized by two alternative metrics: β is the fraction of the street for which there is a gap on either one or both sides, and β' is the average fraction of each side of the street that is a gap. A gap is defined as an opening between buildings where there is no third building within 10 meters of that opening. Two minimum-squared-error predictors were fit to the nine street measurements of α using two free parameters where the estimated α is

$$\hat{\alpha} = 3.2\beta + 1.5. \tag{2}$$

The raw rms residual error in $\hat{\alpha}$ is $\sigma_\alpha = 0.27$, which increases to 0.31 after correcting by a factor of $\sqrt{9/7}$ to reflect the fact that two coefficients in (2) and (3) were used to fit 9 unknowns. The metric β' performs less well, where:

$$\hat{\alpha}' = 5.3\beta' + 1.5 \tag{3}$$

and the corrected rms error is is 0.53. If an optimum linear combination of the two metrics is used, the observed 0.22 rms error for α becomes 0.27 when corrected for three fit parameters. Fig. 5 displays α where $2 < \alpha < 5$. The advantage of the metric β is that it correctly predicts large losses if one side of the street is without buildings for a considerable distance.

One rationale for these predictive models is that waveguide-like ray-tracings suggest small uniformly distributed gaps would produce path losses of: $L \cong k'(r/w)^{-b} = kr^{-\alpha}$, where k' and b are constants, w is the street width, and $\beta = \text{sum}(\Sigma)$ of gap widths/street length. This result sug-

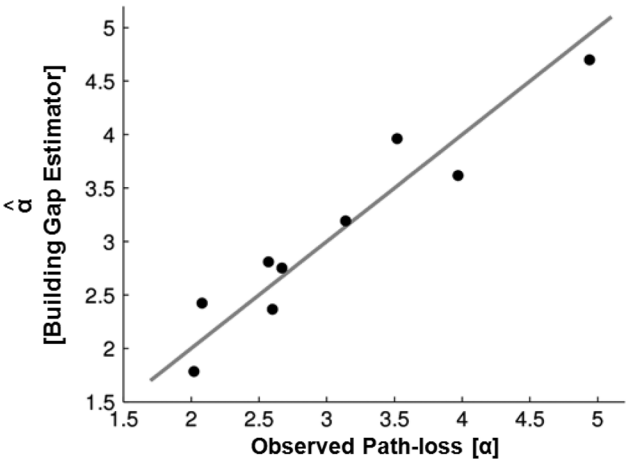

Fig. 5. Relationship between observed path-loss coefficients (α) measured over nine urban streets and estimations utilizing the building-gap-driven estimator of Eqn. (2). The raw standard deviation is 0.27, and becomes 0.31 after correction by $\sqrt{9/7}$.

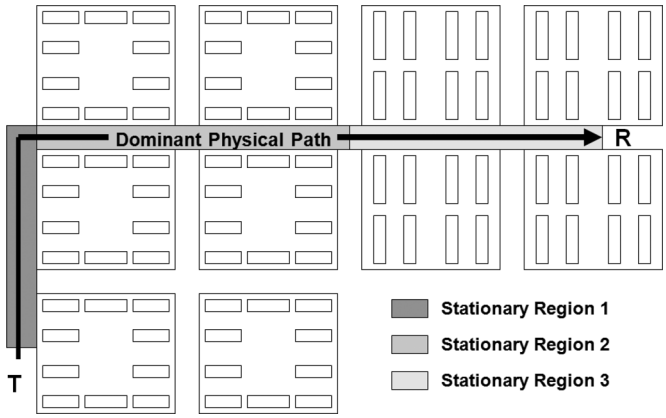

Fig. 6. Path-loss model for a street environment that divides into homogeneous subregions characterized by single values of α.

gests that simple measurable local environmental parameters can be used to improve empirical path-loss models while remaining generally more practical than ray-tracing methods.

These experiments also characterize the fixed power loss (C), due mostly to propagation around corners. Corner loss was defined as the increase in received power when the horizontally isotropic transmitting antenna was moved a relatively minor distance from its occluded location around a corner to a line-of-sight position within the long street. For the 10 corners measured, the associated corner losses had an empirical mean and standard deviation of 40 dB and 5.5 dB, respectively. This is quite consistent with prior measurements for urban intersections [13]. Ray tracing suggests transmission around our observed urban corners was dominated by reflections from building walls rather than by diffraction at vertical discontinuities, which typically have much smaller cross-sections. Two of these ten cases exhibited corner losses approximately 10 dB higher than the average of the remaining corners. These were the only two intersections where the buildings near the corner were constructed primarily with wood (residential houses). In contrast the other intersections had buildings made mostly of brick and concrete cinder block. The dielectric constants for wood or brick suggest that 10–15 dB might be lost due to a single reflection near normal incidence (less at grazing incidence), and that the rest of the nominal 40-dB corner loss might result because the low-loss rays propagating nearly parallel to the first street will initially reflect from corner buildings on the far side of the cross-street at angles that are more nearly normal to the building surfaces; most of the residual 25–30 dB corner loss could then result from the conversion of these initial high-loss modes to lower-loss rays and modes propagating more nearly parallel to the second street. Wood shingles and siding introduce additional loss because they slope several degrees upward and deflect incident rays toward the sky.

In addition, some of the observed variance in corner loss is due to the random placement of the transmitter on the left or right sides of the street, which determines the fraction of rays that can be reflected around the corner toward the receiver; this fraction might vary 2–5 dB for the observed geometries. For the two high-loss corners both the wood-siding and wrong-side-of-street effects were present. These random materials and geometric contributions to corner losses account for a large fraction of the observed standard deviation of 5.5 dB. The high average loss per corner also suggest that only those paths with the minimum number of corners are likely to dominate the multipath propagation routes between any two points; it requires the sum of 10,000 incoherent paths in order to compensate for the 40-dB nominal advantage of a route with one fewer corners.

IV. Path-Loss Model

Consider the communications link illustrated in Fig. 6, where the transmitter and receiver are separated by approximately five blocks and a single one-corner propagation path probably dominates since all alternative paths require propagation around at least two additional corners, each corner having an expected mean loss of 40 dB. The total path loss can be estimated in five steps: 1) determine the dominant physical paths; 2) partition the dominant paths into homogeneous regions characterized by single values of α; 3) estimate α for each homogeneous region using β; 4) estimate the fixed losses associated with each transition between homogeneous regions; and 5) sum the losses along all dominant paths to yield the net path loss between the two nodes.

One path clearly dominates the case shown in Fig. 6, but if the transmitter were moved to the middle of a block on a street in Fig. 6 running left-right, there would be many paths having two corners, and the path loss might increase by roughly 40 dB to account for the extra corner, but then decrease by perhaps 10 dB because there would be perhaps $\mathrm{n} = 10$ paths adding incoherently with useful strength. Partitioning the path illustrated in Fig. 6 into three regions involves identifying where the metric β changes significantly, and α for each region can be estimated from β using (2). The single corner on the dominant path might add 40 dB to the total path loss, and all other paths can be neglected here because they each introduce two additional high-loss corners. If there were two equal paths, each having 60 dB loss, then both the total incoherent power loss and mean coherent loss would be 57 dB.

A. Performance

To compare the performance of this model to traditional empirical models we simulated street propagation using the following distributions for the path-loss coefficient[1] (α) and corner loss (b)

$$\alpha \sim \mathrm{U}(2,5) \tag{4}$$

$$\mathrm{b} \sim \mathrm{N}(40, 5.5)[\mathrm{dB}]. \tag{5}$$

In addition we assume the distribution of the α estimator to be

$$\hat{\alpha} = \alpha + \mathrm{N}(0, 0.22) \tag{6}$$

which is consistent with the performance observed in Cambridge. For a single-corner link of length d, we estimate the path-loss (PL) to be

$$\mathrm{PL}_{\mathrm{model}} = 10\hat{\alpha}\log_{10}(\mathrm{d}) + \hat{\mathrm{b}}[\mathrm{dB}] \tag{7}$$

where

$$\hat{\mathrm{b}} = \mathrm{E}[\mathrm{b}] = 40\ \mathrm{dB}. \tag{8}$$

As discussed in Section I, traditional empirical path-loss models are generally linear predictors trained on various environments, e.g. rural, suburban, or urban. For the street environment considered here, the empirical model would use (8) to find the single α that minimizes rms errors in estimated PL over all streets in this reasonably homogeneous neighborhood. This empirical process yields the estimated statistics $(\mathrm{E}[\alpha], \mathrm{E}[b]) = (3.5, 40)$, as pictured in Fig. 7, where the rms errors in predicting path-loss are ten times greater than for the gap-based model for link lengths as short as 100 meters.

V. Path Loss in Air-to-Ground Links

Another common network topology uses air-to-ground links where one end is much higher in elevation than the other, and the channel is dominated by the scattering environment local to the ground node. This section discusses how the path-loss behavior associated with this type of link fits within our model space.

A. Measurements

The receiver antenna array used for the air-to-ground link measurements was identical to that used in the street measurements of Section III; antenna gains were 8 dBi. The transmitting system was mounted 90 m above street level on the roof of the Green Building located at MIT; its antenna gain was 8 dBi. The look-down angle was sufficiently small that this gain was nearly constant over the sampled neighborhoods. Fig. 8 displays an aerial view of the measured links; the transmitter location is indicated by a red dot, and each blue marker corresponds to a single receiver position for which eight independent receiver channels were measured simultaneously. Diverse neighborhoods and physical scenarios were included in the data set.

[1]U(a,b): Uniformly distributed on [a,b]; $\mathrm{N}(\mu, \sigma^2)$: Gaussian with mean μ and variance σ^2.

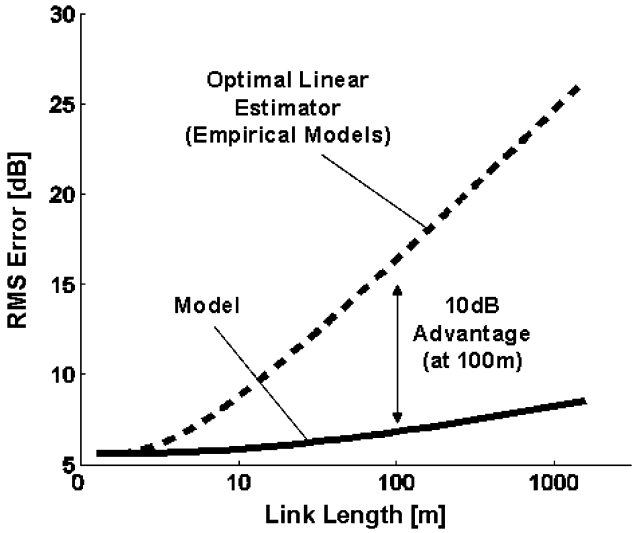

Fig. 7. Performance comparison between our path-loss model and the optimal linear (empirical) model. Our results were obtained by simulating thousands of single corner street environments utilizing (7) and statistics consistent with our measurements for both alpha and corner loss.

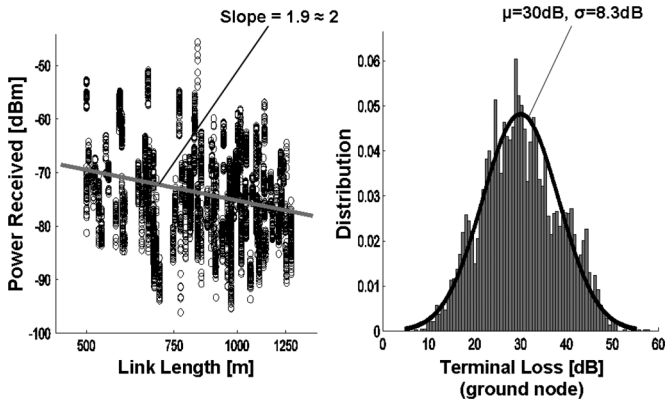

Fig. 8. Left: path losses of these air-to-ground links obtained with transmitter 90 m above street level. Right: distribution of the terminal loss B(dB) incurred near the ground for the tower measurements taken in Cambridge, Massachusetts. The superimposed Gaussian curve suggests this terminal loss ensemble is approximately log-normal.

Fig. 4 displays a scatter plot of link length versus power received (dBm) for each air-to-ground channel measurement. Since the regression line has a negative slope of ∼1.9, the power received decreases approximately as the square of the link length. This is expected since the transmitter sits well above all surrounding buildings that might affect propagation. The standard deviation from the best-fit line is 8.3 dB, as shown in Fig. 8; this scatter is attributed to terminal loss near the ground, which has a mean of 30 dB.

B. Model

Air-to-ground links form a special case within our path-loss model and can be generally broken into two segments: 1) a long line-of-sight (LOS) segment that links the high end of the link to the neighborhood where the low-elevation end is located, and 2) the scattering segment at the low end as illustrated in Fig. 9.

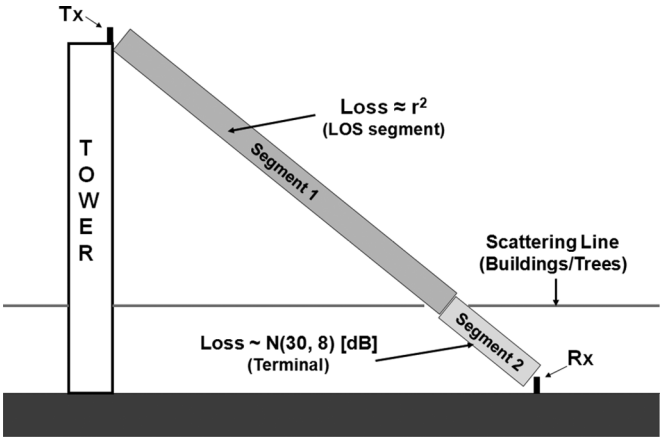

Fig. 9. Air-to-ground links represent a special case of our path-loss model that include two stationary sub-regions corresponding to the propagation path above and below the scattering line at the ground link. While path-loss characteristics should remain stable for segment 1, the statistics of the fixed loss associated with the ground link will vary by environment.

The wave intensity in the LOS segment decays as r^2, so the additional "terminal" loss (dB) at the low-elevation scattering end can be determined by subtracting $10\log_{10}(G_t/4\pi r^2)$ from the total observed link loss (dB), where G_t is the 8-dB gain of the transmitting antenna. The terminal loss for the links illustrated in Fig. 8 was observed to be Gaussian with a standard deviation from the best-fit line of 8.3 dB. This 8.3-dB uncertainty arises from scattering from trees and buildings near the ground and significantly affects link capacity. The model path loss estimate therefore is

$$\mathrm{PL} = 20\log_{10}\mathrm{r} + \mathrm{B}[\mathrm{dBm}] \tag{9}$$

where r is the LOS path length [m] and B is the additional random terminal loss which, for this Cambridge data set was $B = 30 \pm 8.3$ dB (rms). This result is consistent with the log-normal fading assumption presented by others [17], [18]. Future work may suggest simple ways to improve predictions of B based on the character of the local scattering environment.

VI. Conclusion

This paper has shown that satellite images of buildings and of the gaps between them can support useful estimates of the coefficient α in the path-loss model: $(\text{power received})/(\text{power transmitted}) = L = kr^{-\alpha}$ for propagation losses along straight level streets. Two predictors for α were tested over the range $2 < \alpha < 5$; the more successful predictor depended linearly on the fraction β of the street that had a gap on either one or both sides. The residual rms error in predicted values of α was $\sim$0.3 for the nine streets tested.

It was also shown that rms departures of measured losses along single streets from values predicted by the model $L = kr^{-\alpha}$ were typically less than 2 dB when the best-fit value of α for that street was used and when the transmitter was hidden around a corner. This model predicted the loss L for all street measurements with rms errors [dB] for $r > 100$ m that were generally more than 10 dB better than those achieved with a minimum-square-error predictor of L based only on the distance r and the same data set.

In addition, observed corner losses in Cambridge were 40 ± 5.5 dB, consistent with the results of others. Since these corner losses are substantially greater than urban single-street losses, one indicated method for predicting urban path-losses involves identifying those street sequences having the fewest corners, and then determining the gap metrics for those streets using aerial photography. These results also suggest that the most efficient placement of urban street-level wireless terminals is above traffic, below rooftops, and positioned out into street intersections so that only one corner reflection is usually required to reach any address within several rectangular city blocks.

Similarly, air-to-ground links can be modeled as having a line-of-sight component with $\alpha > 2$ (above the local building/tree scattering line), and then an additive Gaussian random component B due to local scattering near the ground-level terminal (empirically $B \approx 30 \pm 8$ dB for Cambridge)

References

[1] J. H. Winters, "On the capacity of radio communication systems with diversity in a Rayleigh fading environment," *IEEE J. Select Areas Commun.*, vol. SAC-5, pp. 871–878, Jun. 1987.

[2] G. J. Foschini and M. J. Gans, "On limits of wireless communications in a fading environment when using multiple antennas," *Wireless Personal Commun.*, vol. 6, pp. 311–335, Mar. 1998.

[3] T. L. Marzetta and B. M. Hochwald, "Capacity of a mobile multiple-antenna communication link in Rayleigh flat fading," *IEEE Trans. Inf. Theory*, vol. 45, pp. 139–157, Jan. 1999.

[4] G. G. Raleigh and J. M. Cioffi, "Spatio-temporal coding for wireless communication," *IEEE Trans. Commun.*, vol. 46, pp. 357–366, Mar. 1998.

[5] D. W. Bliss, A. M. Chan, and N. B. Chang, "MIMO wireless communication channel phenomenology," *IEEE Trans. Antennas Propag.*, vol. 52, no. 8, pp. 2073–2082, Aug. 2004.

[6] E. Bonek, M. Herdin, W. Weichselberger, and H. Ozcelik, "MIMO—Study propagation first!," in *Proc. 3rd IEEE Int. Symp. on Signal Proces. and Inf. Technol. (ISSPIT 2003)*, Dec. 2003, pp. 150–153.

[7] T. Kurner, D. J. Cichon, and W. Wiesbeck, "Concepts and results for 3D digital terrain-based wave propagation models: An overview," *IEEE J. Select Areas Commun.*, vol. 11, pp. 1002–1012, Sep. 1993.

[8] S. Y. Seidel and T. S. Rappaport, "Site-specific propagation prediction for wireless in-building personal communication system design," in *Proc. IEEE 52nd Veh. Technol. Conf.*, Nov. 1994, vol. 43, no. 4, pp. 879–891.

[9] G. E. Athanasiadou, A. R. Nix, and J. P. McGeehan, "A microcellular ray-tracing propagation model and evaluation of its narrow-band and wide-band predictions," *IEEE J. Select Areas Commun.*, vol. 18, pp. 322–335, Mar. 2000.

[10] N. Blaunstein, M. Toeltsch, J. Laurila, E. Bonek, D. Katz, P. Vainikainen, N. Tsouri, K. Kalliola, and H. Laitinen, "Signal power distribution in the Azimuth, elevation and time delay domains in urban environments for various elevations of base station antenna," *IEEE Trans. Antennas Propag.*, vol. 54, no. 10, pp. 2902–2916, Oct. 2006.

[11] T. K. Sarkar, Z. Ji, K. Kim, A. Medouri, and M. Salazar-Palma, "A survey of various propagation models for mobile communication," *IEEE Trans. Antennas Propag.*, vol. 45, no. 3, pp. 51–82, Jun. 2003.

[12] Z. Yun, Z. Zhang, and M. F. Iskander, "A ray-tracing method based on the triangular grid approach and application to propagation prediction in urban environments," *IEEE Trans. Antennas Propag.*, vol. 50, no. 5, pp. 750–758, May 2002.

[13] J. Lee and H. L. Bertoni, "Coupling at cross, T, and L junctions in tunnels and urban street canyons," *IEEE Trans. Antennas Propag.*, vol. 51, no. 5, pp. 926–935, May 2003.

[14] K. R. Schaubach, N. J. Davis, and T. S. Rappaport, "A ray tracing method for predicting path loss and delay spread in microcellular environments," in *Proc. IEEE 42nd Veh. Technol. Conf.*, May 1992, vol. 2, pp. 932–935.

[15] V. Erceg, K. V. S. Hari, M. S. Smith, K. P. Sheikh, C. Tappenden, J. M. Costa, D. S. Baum, and C. Bushue, Channel Models for Fixed Wireless Applications IEEE 802.16 Broadband Wireless Access Working Group, IEEE tech. rep. 802.16.3c-01/29, Jan. 2001 [Online]. Available: http://www.wirelessman.org/tg3/contrib/802163c-01_29.pdf

[16] Y. Okamura, E. Ohmori, and K. Fukuda, "Field strength and its variability in VHF and UHF land mobile radio service," *Rev. Elect. Commun. Lab.*, vol. 16, no. 9–10, pp. 825–873, 1968.

[17] M. Hata, "Empirical formula for propagation loss in land mobile radio services," *IEEE Trans. Veh. Technol.*, vol. VT-29, no. 3, pp. 317–325, Aug. 1980.

[18] Digital Mobile Radio Towards Future Generation Systems COST Action 231, European Co-operation in Mobile Radio Research, European Commission, Brussels, Belgium, Final Tech. Rep. EUR 18957, 1999, E. Damosso, L. M. Correia (eds.).

[19] K. Herring, "Propagation Models for Multiple-Antenna Systems: Methodology, Measurements, and Statistics," Ph.D. dissertation, Dept. Elect. Eng. Comp. Sci., MIT, Cambridge, MA, 2008.

[20] J. Bicket, D. Aguayo, S. Biswas, and R. Morris, "Architecture and evaluation of an unplanned 802.11b mesh network," presented at the Mobicom 2005, Aug. 2005.

[21] T. S. Rappaport, *Wireless Communications: Principles and Practice*. Upper Saddle River, NJ: Prentice Hall, 2002.

[22] D. Tse and P. Viswanath, *Fundamentals of Wireless Communication*. Cambridge, UK: Cambridge Univ. Press, 2005.

Keith T. Herring received the B.S. degree in computer science from the University of Illinois, Urbana-Champaign, in 2003 and the S.M. and Ph.D. degrees in electrical engineering and computer science from the Massachusetts Institute of Technology (MIT), Cambridge, in 2005 and 2008, respectively.

He worked in the Research Laboratory of Electronics (RLE) at MIT from 2003 to 2008, focusing on wireless propagation research. Currently he is a Postdoctoral Associate in the MIT Research Laboratory of Electronics.

Jack W. Holloway received both the S.B. degree in applied mathematics and the S.B. degree in electrical engineering in 2003 and the M.Eng. degree electrical engineering and computer science in 2004, all from the Massachusetts Institute of Technology (MIT), Cambridge.

Previously, he was engaged in Ph.D. work in integrated RF circuit design at the Micro-Technology Lab, MIT. Currently, he is a Second Lieutenant in the United States Marine Corps, currently undergoing training as a Naval Aviator in Corpus Christi, TX.

David H. Staelin (S'59–M'65–SM'75–F'7–LF'04) received the S.B., S.M., and Sc.D. degrees in electrical engineering from the Massachusetts Institute of Technology (MIT), Cambridge, in 1960, 1961, and 1965, respectively.

He joined the MIT faculty in 1965, where he is currently a Professor of electrical engineering and teaches electromagnetics and signal processing. He was the Principal Investigator for the Nimbus E Microwave Spectrometer (NEMS) and Scanning Microwave Spectrometer (SCAMS) experiments on the National Aeronautics and Space Administration's (NASA) Nimbus-5 and Nimbus-6 satellites and a Coinvestigator for the NASA Atmospheric Infrared Sounder/Advanced Microwave Sounding Unit sounding experiment on Aqua, Scanning Multichannel Microwave Radiometer experiment on Nimbus 7, and Planetary Radio Astronomy Experiment on Voyager 1 and 2. Other research has involved estimation, radio astronomy, video coding, milliarc-second optical astrometry, random process characterization, and wireless communications. He is a member of the National Polar-Precipitation Measurement Missions and the NPOESS Preparatory Program (NPP). He was an Assistant Director of the MIT Lincoln Laboratory from 1990 to 2001.

Daniel W. Bliss (M'03) received the B.S.E.E. degree in electrical engineering from Arizona State University, Tempe, in 1989, and the M.S. and Ph.D. degrees in physics from the University of California at San Diego, in 1995 and 1997, respectively.

Currently, he is a staff member at MIT Lincoln Laboratory, Massachusetts Institute of Technology (MIT), Cambridge, in the Advanced Sensor Techniques group. He was employed by General Dynamics from 1989 to 1991, he designed avionics for the Atlas-Centaur launch vehicle and performed research and development of fault-tolerant avionics. As a member of the superconducting magnet group at General Dynamics from 1991 to 1993. He performed magnetic field calculations and optimization for high-energy particle-accelerator superconducting magnets. His doctoral wor,k from 1993 to 1997, was in the area of high-energy particle physics, searching for bound states of gluons, studying the two-photon production of hadronic final states, and investigating innovative techniques for lattice-gauge-theory calculations. Since 1997, he has been employed by MIT Lincoln Laboratory, where he focuses on multiantenna adaptive signal processing and performance bounds, primarily for communication systems. His current research topics include MIMO communication channel phenomenology, space-time coding, information-theoretic bounds for MIMO communication systems, algorithm development for multichannel multiuser detectors (MCMUD), and multiple-input multiple-output (MIMO) radar concepts.